Shuwen Zhou
Jinshuang Liu ✉
Zhaolun Wang
Shaohua Sun

https://doi.org/10.21278/TOF.474045522
ISSN 1333-1124
eISSN 1849-1391

RESEARCH ON DESIGN OPTIMIZATION AND SIMULATION OF REGENERATIVE BRAKING CONTROL STRATEGY FOR PURE ELECTRIC VEHICLE BASED ON EMB SYSTEMS

Summary

The benefits of electromechanical braking (EMB) systems are short response time, high braking efficiency, ease of assembly and easy integration with other electronic control systems. Therefore, a model of an EMB system is developed based on which the braking stability, braking efficiency, and the regenerative braking energy recovery in electric vehicles are investigated. Electric vehicles can effectively increase their driving range by using a rational regenerative braking control strategy. Firstly, a fuzzy regenerative braking control strategy is developed for comparison, and an optimized regenerative braking control strategy is designed based on the NSGA-II algorithm. The technique for order preference by similarity to ideal solution (TOPSIS) is used to comprehensively evaluate the Pareto optimal solution set and to select an optimal solution for the optimization problem. Secondly, a Takagi-Sugeno fuzzy neural network is trained with the optimized discrete data, and then the braking force distribution controller is obtained. Simulink and AVL CRUISE are used to simulate the control strategy. The simulation results for variable intensity braking conditions and cyclic conditions NEDC, FTP75, and CLTC-P show that the optimized control strategy outperforms the fuzzy control strategy in braking stability and braking energy recovery.

Key words: *electromechanical brake; pure electric vehicle; regenerative braking control strategy; genetic algorithm; fuzzy neural network*

1. Introduction

The automotive industry relies heavily on oil resources accelerating the depletion of natural resources. Exhaust gases emitted by automobiles also cause severe damage to the environment [1]. Therefore, electric vehicles have gained in popularity due to their zero-emissions driving and small energy losses [2]. However, the development of the electric vehicle market is still restricted, hence the core technical problems that restrict this growth need to be solved [3]. The primary problem to be solved is driving range [4]. By utilizing the braking energy recovered by the regenerative braking system, the driving range of pure electric vehicles can be effectively increased.

Many scholars have studied the EMB braking technology. Saric et al. [5] developed a clamping force estimation model based on dynamic stiffness relationships and a torque balance approach and used the maximum likelihood estimation to fuse the outputs of two independent models. Ki et al.[6] proposed a clamping force estimation method based on the information about the rotor position in the motor and the hysteresis characteristics of the executive components in the EMB system, which performed better than existing estimation methods. Combining the EMB system with ABS, Zhou et al. [7] proposed a vehicle control strategy based on the slip rate. Jo et al. [8] proposed an adaptive proportional-integral-derivative (PID) control strategy for the EMB clamping force control. The EMB system tracks the clamping force quite well and maintains the ideal braking clearance. Haggag et al. [9] proposed an optimal control tracking strategy for the EMB system, which tracks brake pedal commands and brake deceleration effectively protecting the braking mechanism from high currents.

Designing regenerative braking control strategies has emerged as an important research orientation to solve the driving range problem. Grandone et al. [10] built a real-time braking control model considering the change in axle load and wheel slip. The braking control strategy based on this model can achieve a balance between friction braking and motor braking. Rajendran et al. [11] designed an intelligent sliding mode control strategy, which can well track the expected slip rate under emergency braking conditions. This strategy allows for the recycling of braking energy as much as possible while ensuring battery safety. Considering the motor power, the anti-lock braking system and the battery operating characteristics together, Oleksowicz et al. [12] developed three regenerative braking control strategies and conducted a simulation study. Khastgir et al. [13] proposed a regenerative braking control strategy that uses regenerative braking force for front wheels. With this strategy, the vehicle can recover approximately 30% of the braking energy. Maiad et al. [14] proposed a regenerative braking control strategy based on the fuzzy set theory. The strategy improves the braking energy recovery rate by regarding the vehicle acceleration, acceleration rate of change and road gradient as input variables and the proportion of regenerative braking force as output variables.

The issue of driving range is an important factor restricting the development of pure electric vehicles [15]. The researchers working on batteries are faced with a dilemma about the need to develop the technology further and the lack of money and safety. Therefore, this paper studies the regenerative braking control strategy to make full use of the advantages of the regenerative braking system to ensure braking stability and improve the driving range of electric vehicles.

2. Braking force distribution requirements

The maximum torque of the electric motor is 240 N·m, the maximum power is 75 kW, and the maximum speed is 7500 r/min. The working voltage of the lithium iron phosphate battery pack is 320 V, and the capacity is 59.85 Ah.

The force diagram of the vehicle braking is simplified, as shown in Figure 1:

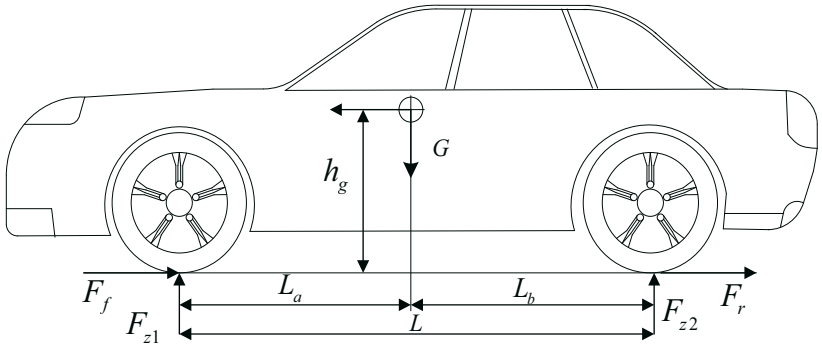

Fig. 1 Force diagram of vehicle during braking

The basic parameters of the selected vehicle are shown in Table 1.

Table 1 Vehicle parameters

Parameter	Value	Unit
Curb weight	1250	kg
Full load weight	1580	kg
Centroid height	0.52	m
Wheelbase	2.605	m
Distance from the centroid to the front axle	1.17	m
Distance from the centroid to the rear axle	1.435	m
Wheel rolling radius	0.301	m
Rolling resistance coefficient	0.015	-
Windward area	1.97	m^2
Wind resistance coefficient	0.34	-

Before designing a braking energy recovery strategy, the requirements for the braking force distribution in electric vehicles need to be analyzed so that the strategy can meet the relevant regulations [16]. The normal reaction force of the ground to the front and rear wheels is obtained according to the principle of moment balance as:

$$\begin{cases} F_{zf} = \dfrac{G}{L}(L_b + zh_g) \\ F_{zr} = \dfrac{G}{L}(L_a - zh_g) \end{cases}, \tag{1}$$

where F_{zf} and F_{zr} are the normal reaction forces of the ground to the front and rear wheels; G is the gravity of the vehicle; L is the wheelbase; L_a and L_b are the distances from the centroid to the front and rear axles; z is the braking strength; h_g is the height of the centroid.

During vehicle braking, simultaneous locking of the front and rear wheels is in a stable condition. For different φ values of the road surface, the distribution curve of the front and rear wheel braking force is called the ideal braking force distribution curve (I curve), which satisfies the following relationship:

$$\begin{cases} F_f + F_r = \varphi G \\ \dfrac{F_f}{F_r} = \dfrac{L_b + \varphi h_g}{L_a - \varphi h_g} \end{cases} \tag{2}$$

$$F_r = \frac{1}{2}\left[\frac{G}{h_g}\sqrt{L_b^{\,2} + \frac{4h_g L}{G}F_f} - \left(\frac{GL_b}{h_g} + 2F_f\right)\right], \tag{3}$$

where φ is the road adhesion coefficient; F_f and F_r are the ground frictions of the front and rear axles.

When the braking force distribution points are distributed below the I curve, there is no danger of the rear wheels locking up first. The closer the distribution point to the I curve, the better the braking stability and the more fully utilized the ground adhesion conditions.

The f line corresponding to a certain value of φ when the brakes are applied can be expressed as:

$$\begin{cases} F_f = \varphi\dfrac{G}{L}(L_b + zh_g) \\ Gz = F_f + F_r \end{cases} \tag{4}$$

Arranging Eq. (4), the relationship between the rear wheel braking force and the front wheel braking force is:

$$F_{\mathrm{r}}=\frac{L-\varphi h_{\mathrm{g}}}{\varphi h_{\mathrm{g}}}F_{\mathrm{f}}-\frac{GL_{\mathrm{b}}}{h_{\mathrm{g}}} \tag{5}$$

Similarly, the r line corresponding to a certain value of φ when the brakes are applied can be expressed as:

$$\begin{cases}F_{\mathrm{r}}=\varphi\dfrac{G}{L}(L_{\mathrm{a}}-zh_{\mathrm{g}})\\ Gz=F_{\mathrm{f}}+F_{\mathrm{r}}\end{cases} \tag{6}$$

Arranging Eq. (6), the braking force distribution relationship between the front and rear wheels on the r line is:

$$F_{\mathrm{r}}=\frac{-\varphi h_{\mathrm{g}}}{L+\varphi h_{\mathrm{g}}}F_{\mathrm{f}}+\frac{\varphi GL_{\mathrm{a}}}{L+\varphi h_{\mathrm{g}}} \tag{7}$$

ECER13 regulations stipulate that to ensure the stability and safety of the braking process of a vehicle, for all vehicles between φ = 0.2~0.8, the braking strength is required to meet the following requirement:

$$z\geq 0.1+0.85(\varphi-0.2) \tag{8}$$

The curve in the part of $F_r \geq 0$ is used as the boundary line specified by the Economic Commission for Europe (ECE) regulations and is represented as follows:

$$\begin{cases}F_{\mathrm{f}}=\dfrac{z+0.07}{0.85}\dfrac{G}{L}(L_{\mathrm{b}}+zh_{\mathrm{g}})\\ F_{\mathrm{r}}=Gz-F_{\mathrm{f}}\end{cases} \tag{9}$$

In general, the utilization coefficient of adhesion of the front axle of the vehicle should be greater than the utilization coefficient of adhesion of the rear axle. When $z=0.3\sim0.4$, the utilization coefficient of attachment of the front axle is allowed to be smaller than that of the rear axle as long as the utilization coefficient of attachment of the rear axle is not greater than $z+0.05$.

3. EMB system model

3.1 EMB system mathematical model

The EMB model is mainly composed of an executive motor model, a deceleration and torque-increasing mechanism model, a motion conversion mechanism model, and a load mechanism model. Each part of the EMB system requires a mathematical model.

The brushless DC torque motor is selected as the executive motor of the EMB system. Its mathematical model is as follows:

$$U_{\mathrm{a}}=E_{\mathrm{a}}+L_{\mathrm{a}}\frac{\mathrm{d}I_{\mathrm{a}}}{\mathrm{d}t}+I_{\mathrm{a}}R_{\mathrm{a}} \tag{10}$$

$$E=K_{\mathrm{e}}\frac{\mathrm{d}\theta_{\mathrm{m}}}{\mathrm{d}t}=K_{\mathrm{e}}\omega_{\mathrm{m}} \tag{11}$$

$$T_{\mathrm{m}}=K_{\mathrm{t}}I_{\mathrm{a}} \tag{12}$$

$$J_{\mathrm{m}}\frac{\mathrm{d}^2\theta_{\mathrm{m}}}{\mathrm{d}t^2}=T_{\mathrm{m}}\text{-}T_{\mathrm{f}}\text{-}T_{\mathrm{L}}\,, \tag{13}$$

where U_a is the motor armature voltage; I_a is the motor armature current; R_a is the motor armature resistance; L_a is the motor armature inductance; K_e is the motor back emf coefficient; θ_m is the motor rotation angle; J_m is the equivalent moment of inertia; T_m is the motor electromagnetic torque; T_f is the motor friction torque; T_L is the motor load torque, N·m; K_t is the motor torque coefficient.

The Stribeck friction model is selected as the friction model of the motor. The planetary gear mechanism is selected as the deceleration and torque-increasing mechanism of the EMB actuator, which is responsible for amplifying and transmitting the torque output by the EMB actuator motor to the ball screw. The output angle and the linear displacement generated when the ball screw is pushed can be expressed as:

$$\theta_{\mathrm{n}} = \theta_{\mathrm{m}} / i_{\mathrm{z}} \tag{14}$$

$$x_{\mathrm{n}} = \frac{S_{\mathrm{n}}}{2\pi}\theta_{\mathrm{n}} = \frac{S_{\mathrm{n}}}{2\pi i_{\mathrm{z}}}\theta_{\mathrm{m}}, \tag{15}$$

where T_s is the maximum static friction torque; T_c is the coulomb friction torque; ω_s is the Stribeck velocity; B_v is the viscous friction coefficient; δ is the empirical constant.

As a motion conversion mechanism, the ball screw is used to convert the rotary motion of the upper-level mechanism into the linear motion of the lead screw to generate the pressing force for the brake caliper to press the brake disc. Simplifying the roller screw into a "mass-spring-damping" system, the corresponding mathematical model is as follows:

$$\Delta x = x_{\mathrm{n}} - x_{\mathrm{s}} \tag{16}$$

$$F_{\mathrm{d}} = M_{\mathrm{s}} \frac{\mathrm{d}^2 \Delta x}{\mathrm{d}t^2} + K_{\mathrm{a}} \Delta x + B_{\mathrm{e}} \frac{\mathrm{d}\Delta x}{\mathrm{d}t} \tag{17}$$

$$\frac{1}{K_{\mathrm{a}}} = \frac{1}{K_{\mathrm{b}}} + \frac{1}{K_{\mathrm{s}}} \tag{18}$$

$$x_{\mathrm{s}} = x_{\mathrm{z}} + x_{\mathrm{c}}, \tag{19}$$

where F_d is the driving force of the ball screw; M_s is the equivalent mass of the friction plate and the ball screw; x_s is the linear displacement of the screw; B_e is the damping coefficient of the system; K_a is the equivalent axial stiffness of the system; K_b is the bearing stiffness; K_s is the axial stiffness of the screw; x_z is the braking clearance; x_c is the deformation of the friction plate.

The test results of the related research show that the clamping force exerted on the brake disc is a cubic polynomial of the deformation of the friction lining. The brake disc clamping force is expressed as:

$$F_{\mathrm{cl}} = k_1 x_{\mathrm{c}}^{\ 3} + k_2 x_{\mathrm{c}}^{\ 2} + k_3 x_{\mathrm{c}}, \tag{20}$$

where k_1, k_2, and k_3 are the clamping force coefficients.

The braking torque output of the floating caliper disc brake model is expressed as follows:

$$T_{\mu} = 2\mu F_{\mathrm{cl}} R_{\mathrm{b}} \tag{21}$$

where μ is the friction coefficient of the brake disc; R_b is the effective friction radius of the brake disc.

3.2 EMB system response control

In this paper, a clamping force-velocity-current triple closed-loop PID control strategy is used to control the response of the EMB braking system. A particle swarm algorithm is used to determine optimal parameters of the PID control system. To verify the effectiveness of the EMB controller, a step signal and a high-frequency sinusoidal signal are fed to the control system. It is required that the clamping force ring can respond quickly to the input quantity, the overshoot should not exceed 5%, and the braking gap elimination time should not exceed 0.1s.

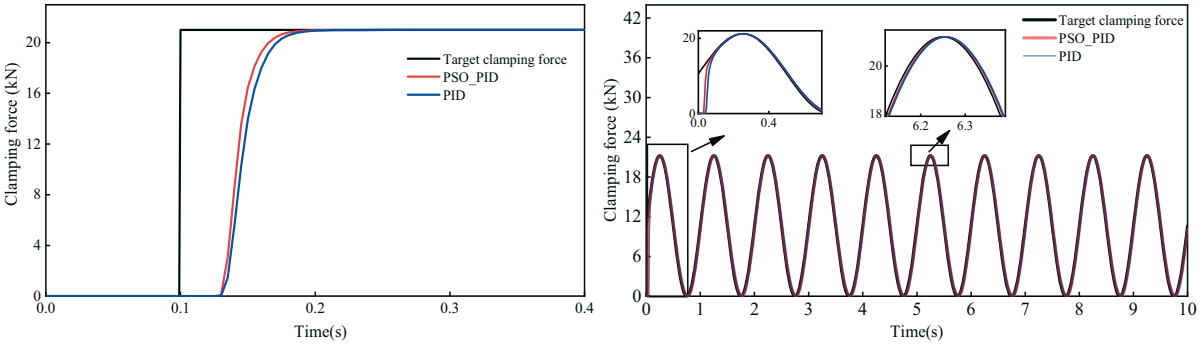

Fig. 2 (a) Tracking of clamping force under emergency braking condition
(b) Tracking of clamping force under continuous braking condition

By comparing the step response curves of the EMB system before and after particle swarm optimization (PSO), it can be seen that the EMB system under the unoptimized PID control eliminates the braking gap after 0.03 s, the motor begins to enter the locked-rotor state and completely tracks the target clamping at 0.215 s force. The EMB system controlled by the PSO_PID controller eliminates the braking gap in 0.03 s and fully tracks the desired clamping force in 0.205 s with almost no overshoot. The results show that both controllers can realize the fast-tracking of the target clamping force exerted by the EMB system, and the response speed and accuracy of the PID controller optimized are better when the PSO is applied.

The controller enables an efficient tracking of the sinusoidal response to the desired clamping force. When the EMB is activated for the first time, it can quickly eliminate the braking gap (the time to eliminate the braking gap is less than 0.1 s). After eliminating the braking gap, the actual clamping force of the EMB basically coincides with the expected clamping force, which can meet the braking requirements. After the clearance is eliminated and partial amplification results of about 6.25 s are observed, the response speed of the EMB controlled by the PSO_PID controller is faster, and the actual clamping force output is closer to the target clamping force. The above results verify that the PSO_PID controller designed in this paper has an ideal response speed and accuracy when compared to the PID controller operating under continuous multiple braking conditions.

4. Fuzzy control strategy based on braking safety area

The braking force distribution process during the vehicle braking is difficult to control by applying traditional mathematical modelling ideas. Fuzzy control does not require mathematical modelling and completes logical thinking decisions through fuzzy reasoning [17]. Therefore, a strategy based on the fuzzy mathematical theory can reasonably control the process of distributing the braking force of the regenerative braking system in electric vehicles [18]. The braking force distribution strategy designed based on the fuzzy control theory is shown in Figure 3.

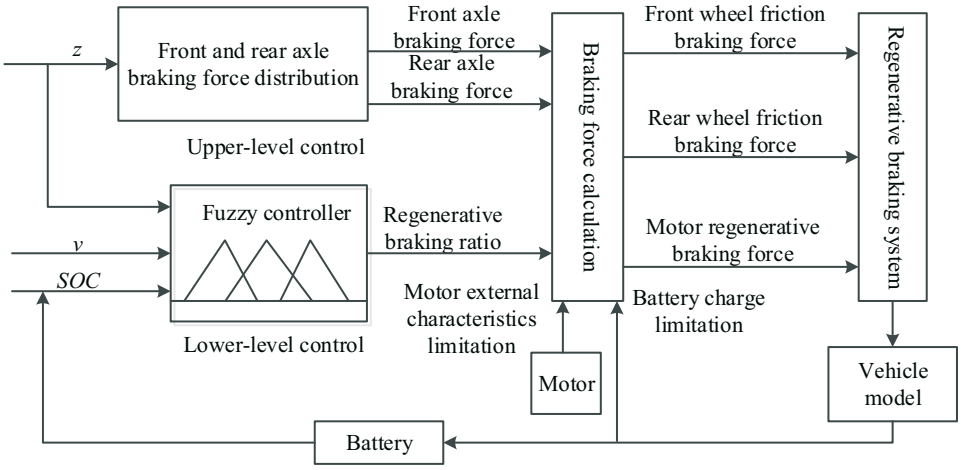

Fig. 3 Regenerative braking control strategy based on fuzzy set theory

The control strategy is split into two parts: the top-level controller and the bottom-level controller. Considering the braking stability and safety of the whole vehicle, the distribution point of the vehicle braking force in this paper is limited to a polygonal area, which is called the braking safety area [19]. The top-level controller is responsible for generating the front and rear axle brake force distribution control lines within the braking safe area. The bottom-level controller uses the fuzzy controller to create the regenerative braking ratio. In the top-level controller, the control line is divided into two cases in accordance with the different road attachment coefficients, and the design ideas are shown in Figure 4.

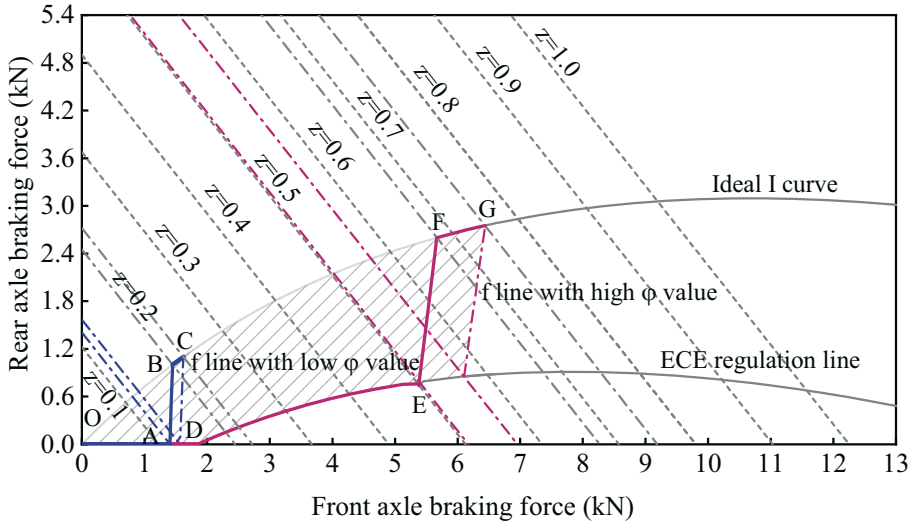

Fig. 4 Front and rear axle braking force distribution control line

When the road adhesion coefficient is small, the OABC curve is the braking force distribution control line at this time. When the braking intensity is less than point A, the braking force is provided by the front axle only (section OA); when the braking intensity increases, the braking force is provided by both the front and rear wheels (section AB). In the figure, the front axle braking force on the AB line is 90% of the f line of equal braking intensity. When the braking intensity is greater than point B, the braking force is distributed according to the I curve until the braking intensity increases to the current road adhesion coefficient. When the road adhesion coefficient is large, the ODEFG curve is the braking force distribution control line. The DE section coincides with the ECE line distributing more braking force to the front axle. The other braking sections are the same as at small adhesion coefficients.

The fuzzy controller has three inputs: velocity, state of charge (SOC), and braking intensity, and the output is the ratio of regenerative braking. According to the theoretical analysis and practical experience, the corresponding fuzzy rules are formulated [20].

5. Regenerative braking control strategy based on multi-objective optimization

5.1 Objective function and constraints

The conventional braking zone is the area of the vehicle where braking is frequent, and the motor is capable of energy recovery in this zone most of the time. This section focuses on the braking force distribution in this area.

The main purpose of the optimization in this paper is to distribute the braking force effectively and reasonably according to the real-time signal obtained from the vehicle to achieve a reasonable balance between the braking stability of the vehicle and the effect of the braking energy recovery. Problems with contradictions among multiple objectives are called multi-objective optimization problems [21]. In this paper, the front and rear axle braking force distribution coefficients and the regenerative braking ratio are selected as design variables for optimization.

There are two optimization objectives in this paper. The objective function that characterizes the braking stability is to use the closeness of the adhesion coefficient to the braking intensity, namely:

$$\min J_1 = \sqrt{\sum (\varphi_i - z)^2} \tag{22}$$

$$\begin{cases} \varphi_{\mathrm{f}} = \dfrac{F_{\mathrm{bf}}}{F_{\mathrm{zf}}} = \dfrac{z\beta L}{L_{\mathrm{b}} + h_{\mathrm{g}} z} \\ \varphi_{\mathrm{r}} = \dfrac{F_{\mathrm{br}}}{F_{\mathrm{zr}}} = \dfrac{L(1-\beta)z}{L_{\mathrm{a}} - h_{\mathrm{g}} z} \end{cases} \tag{23}$$

After arranging Eqs. (12) and (13), the objective function representing braking stability is obtained as:

$$\min J_1 = \sqrt{\left(\frac{z\beta L}{L_{\mathrm{b}} + h_{\mathrm{g}} z} - z\right)^2 + \left(\frac{L(1-\beta)z}{L_{\mathrm{a}} - h_{\mathrm{g}} z} - z\right)^2} \tag{24}$$

The braking energy recovery efficiency is chosen as the objective function to characterize the degree of the braking energy recovery, namely:

$$\min J_2 = \frac{E_{\mathrm{reg}}}{E_{\mathrm{brake}}} = \frac{\int_0^t T_{\mathrm{reg}} \omega(t) \eta_{\mathrm{m}} \mathrm{d}t}{\frac{1}{2} m (v_t^{\,2} - v_0^{\,2})} \tag{25}$$

$$T_{\mathrm{reg}} = \frac{mgzr\beta K_{\mathrm{z}} \eta_{\mathrm{t}}}{i}, \tag{26}$$

where $\omega(t)$ is the speed of the motor at time t; E_{reg} is the energy recovered by the motor regenerative braking; E_{brake} is the total braking energy; η_m is the power generation efficiency; T_{reg} is the motor regenerative braking torque; v_0 is the initial vehicle speed; v_t is the final vehicle speed.

In the process of automobile regenerative braking, the distribution of braking force is affected by many factors. These factors constitute the constraints of the multi-objective optimization. The main influencing factors of regenerative braking [22] are as follows:

(1) Restrictions on the external characteristics of the motor

$$F_{\mathrm{m\_max}} \le \begin{cases} T_{\mathrm{m\_max}} i / r\eta_{\mathrm{t}} & n \le n_{\mathrm{e}} \\ 9550 P_{\mathrm{m\_max}} i / nr\eta_{\mathrm{t}} & n > n_{\mathrm{e}} \end{cases}, \tag{27}$$

where n is the current speed of the motor; $F_{\mathrm{m\_max}}$ is the maximum regenerative braking force; T_{m_max} is the maximum braking torque of the motor; P_{m_max} is the maximum braking power of the motor.

(2) Limitation of battery charging characteristics

In order to prevent overheating and power loss caused by the low battery SOC and overcharging of the battery caused by the high battery SOC, the charging current of the regenerative braking system shall not override the maximum charging current of the battery pack, so the following constraints are introduced:

$$F_{\mathrm{m\_max}} \le \frac{9.55\xi P_{\mathrm{c\_max}} i}{\eta_{\mathrm{t}}\eta_{\mathrm{m}} nr} = \frac{9.55\xi I_{\mathrm{bat\_max}} (U(\sigma) + I_{\mathrm{bat\_max}} R_0) i}{\eta_{\mathrm{t}}\eta_{\mathrm{m}} nr} \tag{28}$$

where $P_{\mathrm{c\_max}}$ is the maximum charging power of the battery; $I_{\mathrm{bat\_max}}$ is the maximum charging current; $U(\sigma)$ is the battery open circuit voltage; σ is the battery SOC value; ξ is the limiting factor to prevent battery overcharge; when the SOC value is greater than 0.9, ξ is 0; when the SOC value is less than 0.9, ξ is 1.

(3) Restrictions of the ECE braking regulations

The constraints constituted by the ECE braking regulations are as follows:

$$\begin{cases} \varphi_f > \varphi_r \quad 0 < z < 1 \\ \varphi_f \le \varphi_r 0.3 < z < 0.4 \; and \; \varphi_r \le z + 0.05 \\ \varphi_f, \varphi_r \le (z + 0.07)/0.850.1 \le z \le 0.6 \end{cases} \tag{29}$$

By substituting the expressions of φ_f and φ_r about the design variable β into Eq. (29) Eq. (30) can be obtained:

$$\begin{cases} 0 \le \beta \le 10 \le z \le 1 \\ \beta > \frac{L_b + zh_g}{L} \quad 0 < z < 0.3 \text{ or } 0.4 < z < 1 \\ \beta \ge 1 - \frac{(z+0.05)(L_a - zh_g)}{zL} 0.3 \le z \le 0.4 \\ \beta \le \frac{(z+0.07)(L_b + zh_g)}{0.85zL} 0.1 < z < 0.568 \\ \beta \le \frac{0.75(L_b + zh_g)}{zL} 0.568 \le z \le 0.75 \end{cases} \tag{30}$$

The braking safety zone determined by the above constraints on the regenerative braking force distribution is shown in Figure 5. When $z < 0.1$, the braking force distribution coefficient β is taken as 1. At this time, the braking force of the entire vehicle is provided entirely by the front axle. When $z > 0.75$, β is taken along the ideal I curve. In this paper, the conventional braking range is targeted, i.e., 0.1 < z < 0.75, with β values restricted to the shaded region in the above figure, and the multi-objective optimization is performed for this braking region.

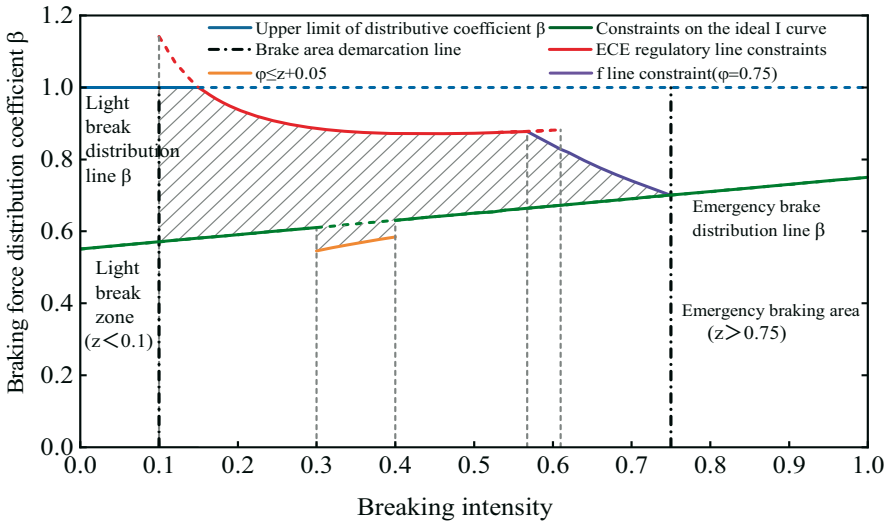

Fig. 5 Range of braking force distribution coefficient

5.2 Pareto optimal solution based on NSGA-II genetic algorithm

The non-dominated sorting genetic algorithm II (NSGA-II) with an elitist strategy is a widely recognized multi-objective optimization algorithm. The algorithm has high computational accuracy and low computational complexity. It can also find a global optimal solution quickly.

The parameters of the NSGA-II algorithm are set as follows: the maximum number of iterations is 200, the optimal front-end coefficient is set to 0.3, and the population size is 200. Different combinations of vehicle speed (0~120km/h), battery SOC (0~80%), and braking intensity (0.1~0.75) are selected as the reference variables for the optimization problem in this paper. The Pareto-optimal solution is to be discovered corresponding to each group of reference variables.

Figure 6(a) presents the braking force distribution coefficient and the regenerative braking rate in each optimal scheme obtained by optimization at the braking intensity of 0.25, the vehicle speed of 50 km/h, and the battery SOC of 50%. In this group of solutions, the force distribution coefficients are in the range from 0.6 to 0.9, which is consistent with the safety range of β when the corresponding braking intensity is 0.25 as shown in the figure. At this time, the braking intensity and the vehicle speed are low, and the braking torque that can be provided by the motor is so large that the braking force of the front axle can be almost completely provided by the motor, so the ratio of regenerative braking is nearly 1.

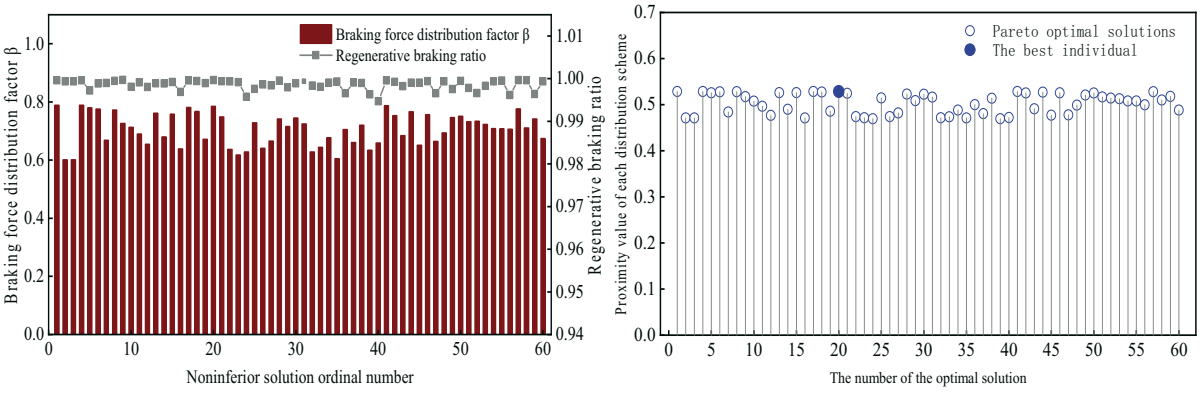

(a) (b)

Fig. 6 (a) Braking force distribution coefficient diagram
(b) Proximity of allocation scheme

In this paper, the TOPSIS evaluation method [23], comparing a set of alternatives and choosing an alternative most similar to the ideal solution, is used to make a final decision on the braking force allocation problem. The closeness value of each solution in the above optimal solution set is obtained, as presented in Figure 6(b). As shown in the figure, among all 60 solutions, the 20th solution has the largest closeness value, so this solution is finally selected as the optimal braking force distribution scheme under this set of reference variables. The optimal braking force distribution scheme for other cases is determined by the same process as above.

5.3 Design of a braking force distribution controller based on fuzzy neural network

The fuzzy neural network is an effective method to solve uncertain and nonlinear system problems without establishing an accurate mathematical model [24]. This control method is widely used in automotive control systems. The adaptive fuzzy inference system based on a neural network can directly adjust the membership function parameters and fuzzy rules according to the training data, thereby improving the performance of the control system [25]. Also, compared with fuzzy systems, the neural network based adaptive fuzzy inference system has strong self-learning and adaptive capabilities [26]. To build an optimized regenerative braking control strategy, a braking force distribution controller based on a Takagi-Sugeno fuzzy neural network is designed. The fuzzy neural network controller is trained and tested by using the optimized discrete data as the controller sample. Figure 7(a) shows a comparison between the braking force distribution coefficient and the regenerative braking ratio of the network output to the actual sample data; Figure 7(b) shows the training error.

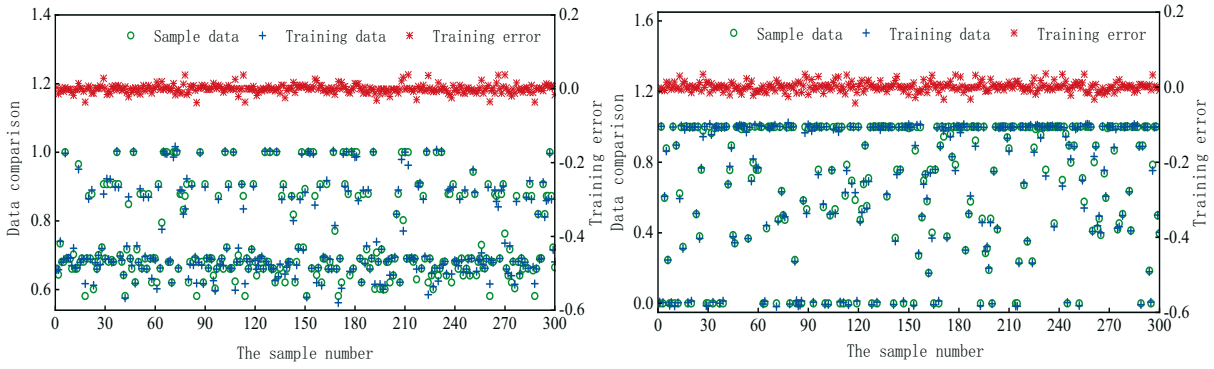

Fig. 7 (a) Training results of front and rear axle braking force distribution coefficient, (b) Training results of regenerative braking ratio

The figure shows that the training error is small for both the braking force distribution coefficients and the ratio of regenerative braking. The learning effect of the trained fuzzy neural network is ideal for the optimized sample data.

5.4 Braking force distribution rules

The braking force distribution rules established in this paper are expressed in the following three parts:

(1) Vehicles in the light braking mode use only the front axle for braking. According to the operating characteristics of the motor and the battery, the data of the maximum braking torque of the motor with the vehicle speed and the SOC of the battery under light braking are calculated and imported into the strategy to obtain a control strategy under the light braking mode.

(2) The vehicle in the conventional braking mode uses a fuzzy neural network controller to accomplish a reasonable distribution of front and rear axle and regenerative braking forces, and to calculate real-time mechanical and electrical torques.

(3) When the vehicle is in the emergency braking mode, the motor regenerative braking is completely withdrawn to ensure the reliability and safety of braking, and the controller distributes the braking force according to the ideal I curve.

6. Simulation and results

The fast and flexible simulation platform AVL CRUISE is suitable for a simulation study of regenerative braking control strategies [27]. Therefore, the effectiveness of the control strategy can be verified by simulating using CRUISE [28] and Simulink together, and the CRUISE solver is called in Simulink. The regenerative braking control strategy based on EMB system and the vehicle co-simulation model are shown in Figure 8.

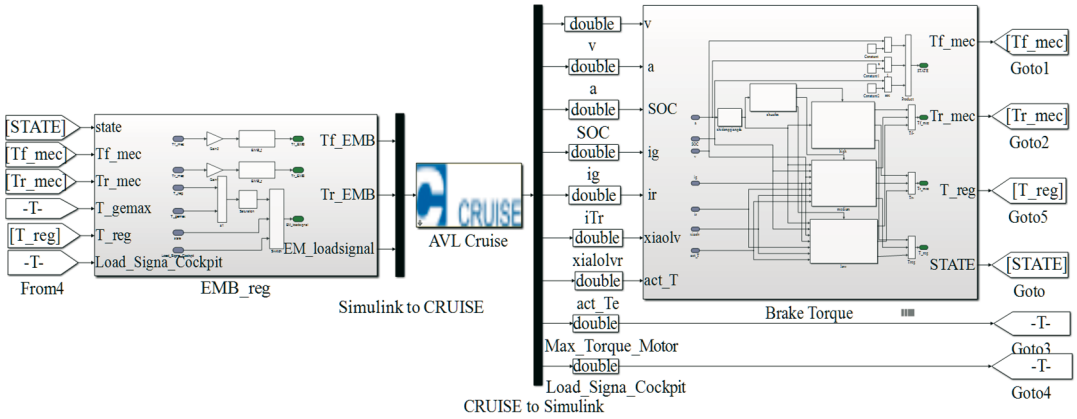

Fig. 8 Joint simulation model of control strategy and a vehicle with EMB system

6.1 Analysis of the simulation of variable strength braking conditions

For the variable-intensity braking conditions designed in this paper, the variation of speed and braking intensity with time is shown in Figure 9(a).

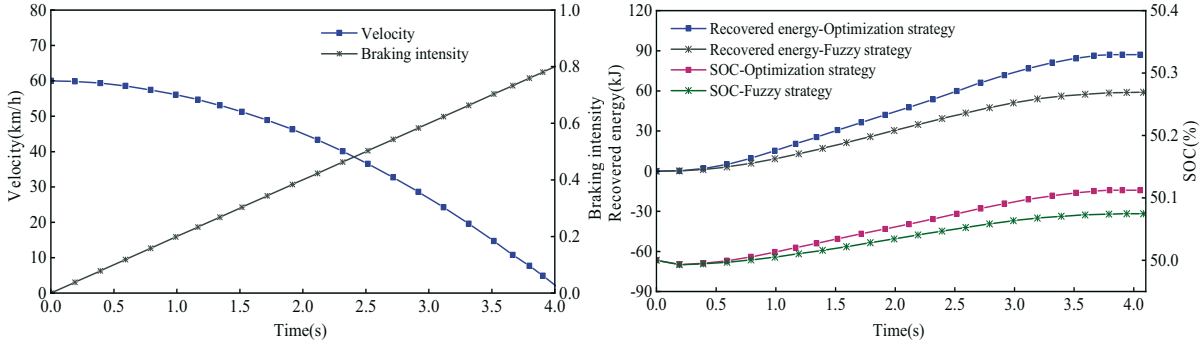

Fig. 9 (a) Variable strength braking conditions
(b) Comparison of SOC and recovered energy of battery under variable intensity conditions

The braking energy recovery in these operating conditions is shown in Figure 9(b). Under the optimized strategy, the battery recovered energy was 87.13 kJ, and the battery SOC increased from the initial 50% to 50.112%. With the fuzzy control strategy, the battery recovered energy was 58.93 kJ, and the battery SOC increased to 50.074%. The optimized control strategy can recover more energy during the variable intensity braking.

The variation curves of the adhesion coefficient utilized by each axis under the two strategies are shown in Fig. 10(a) and Fig. 10(b). As can be seen from the figure, in the range of $0.15 < z < 0.54$, the utilization adhesion coefficients of each axis of the fuzzy control strategy are distributed on the specified line of the ECE regulations, and the braking stability of the

vehicle is poor. In the range of z>0.35, the utilization adhesion coefficient curves of the front and rear axles of the optimized strategy are basically near the braking strength line. This enables the vehicle to obtain a sufficiently large braking effect and better braking stability.

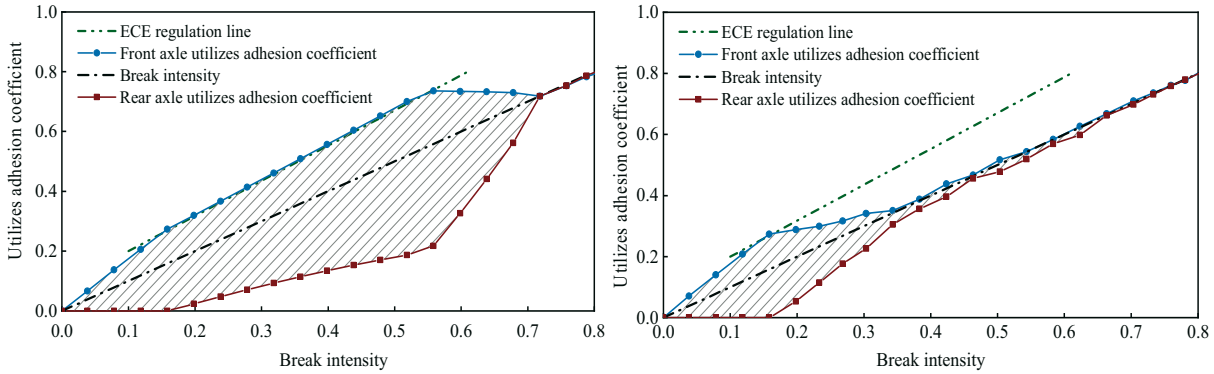

Fig. 10 (a) Adhesion coefficient variation curve using fuzzy control strategy
(b) Adhesion coefficient variation curve using optimized strategy

The braking force distribution curves are presented in Figures 11(a) and 11(b).

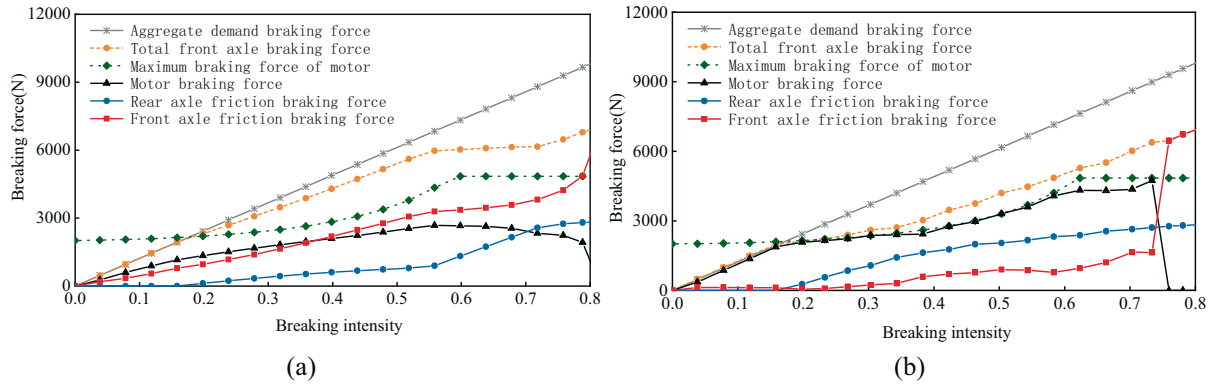

Fig. 11 (a) Braking force distribution curve under fuzzy control strategy
(b) Braking force distribution curve under optimized strategy

The total braking force of the front axle under the fuzzy control strategy has already exceeded the maximum braking force that the motor can provide. As time changes, the speed gradually decreases and the braking intensity gradually increases. The proportion of the regenerative braking output by the controller is reduced, so that the regenerative braking force is always smaller than the maximum braking force of the motor, which makes the energy recovery effect of this strategy poor. Under the optimized control strategy, the regenerative braking force is always close to the maximum braking force line of the motor and, combined with the adhesion coefficient curve, it can be seen that after the braking intensity has reached the value of 0.35, all axes are basically distributed along the ideal I curve.

The comparison of the braking force distribution results between the two strategies shows that the optimized control strategy takes into account the braking demand of the vehicle, the operating characteristics of the motor and battery, and the braking stability. It allows for a more rational distribution of the braking force between the front and rear axles while improving the efficiency of energy recovery.

6.2 Analysis of the simulation of cyclic conditions

The simulation of the regenerative braking system under cyclic conditions can more comprehensively and truly measure the advantages and disadvantages of the regenerative braking control strategy and its influencing factors. In this section, three typical operating cycles

of the New European Driving Cycle (NEDC), the American Federal Test Procedure (FTP-75) and the China Light-duty vehicle test cycle for passenger cars (CLTC-P) are selected for simulation. The initial SOC of the battery under the three driving conditions is 50%.

The simulation results of the NEDC driving conditions are presented in Figure 12.

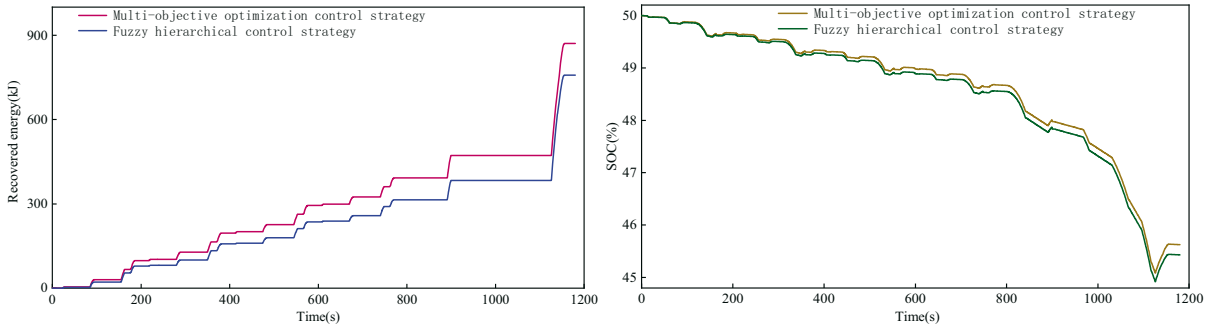

(a) (b)

Fig. 12 (a) Braking energy recovered from battery, (b) Changes in battery SOC

The comparison of the battery SOC and the recovered energy under the two control strategies shows that the energy recovery in the case of the fuzzy control strategy is 758.2 kJ, while the energy recovery in the case of the optimal control strategy is 870.6 kJ, which is 14.7% higher than in the case of the fuzzy control strategy.

The simulation results of the FTP-75 driving conditions are shown in Figure 13.

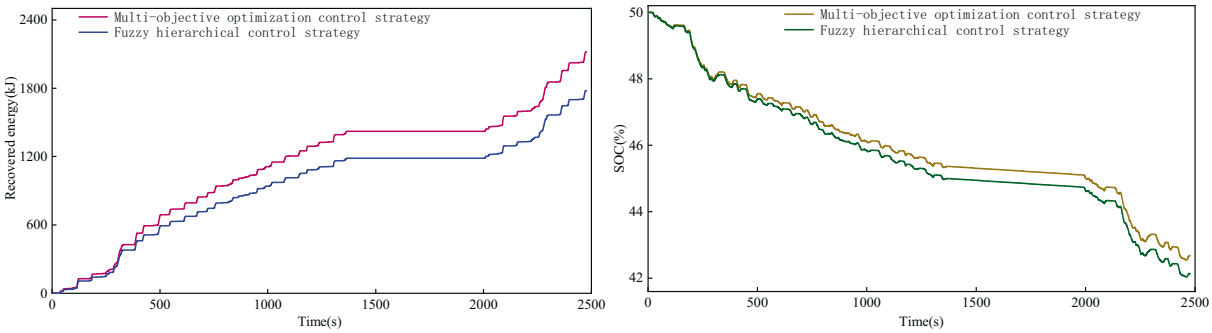

(a) (b)

Fig. 13 (a) Braking energy recovered from battery, (b) Changes in battery SOC

The figure shows that the optimized control strategy has a 19.6% higher energy recovery rate than the fuzzy control strategy.

The simulation results of the CLTC-P conditions are presented in Figure 14.

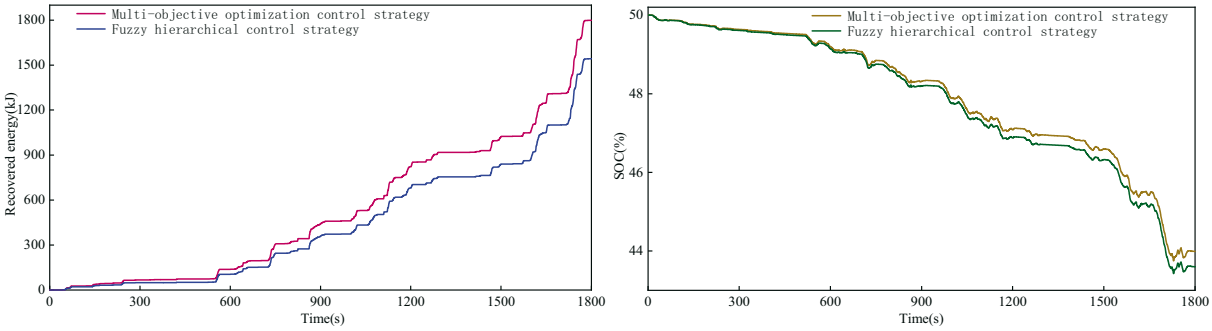

(a) (b)

Fig. 14 (a) Braking energy recovered from battery, (b) Changes in battery SOC

The results show that the braking energy recovered when the optimized control strategy is applied is 1799.6 kJ, which is 16.7% higher than in the case of the fuzzy control strategy, indicating the effectiveness of the optimized strategy under CLTC-P conditions.

The concept of optimum efficiency of braking energy recovery is introduced, and its value is the ratio of the total battery charging energy to the battery discharging energy. It can effectively evaluate the energy recovery effect of cycle conditions. Table 2 shows the simulation results of the efficiency of braking energy recovery of different control strategies under various cycle conditions.

Table 2 Efficiency of braking energy recovery

Cycle conditions	Fuzzy control strategy	Optimized control strategy
NEDC	18.99%	21.92%
CLTC-P	25.53%	29.79%
FTP-75	24.43%	29.11%

The table shows that the optimized control strategy can make the braking energy recovery of the vehicle more efficient, which further verifies the effectiveness and rationality of the optimized control strategy presented in this paper.

7. Conclusion

(1) An EMB system model is developed and validated in this paper. It is introduced into the electric vehicle regenerative braking control strategy to replace the conventional hydraulic braking system. In addition, a fuzzy control strategy based on the braking safety area is designed. Considering the braking stability and braking energy recovery efficiency, a multi-objective optimal control strategy based on the NSGA-II algorithm is proposed. An optimal solution of the optimization problem is found by using the TOPSIS method. By analyzing the optimization data, the rationality of the optimization results is verified.

(2) Fuzzy neural networks are trained by using optimized discrete data to obtain inter-axle braking force and regenerative braking force distribution controllers, and a co-simulation model of the control strategy and the vehicle is developed. Under variable intensity braking conditions, the braking energy recovered by the optimized strategy is 28.2 kJ higher than that of the original fuzzy strategy, and the braking force distribution is more reasonable.

(3) Three representative cycling conditions, NEDC, FTP-75, and CLTC-P, are simulated and analyzed at an initial SOC of 50% of the battery. The results show that under different cycle conditions, the optimized control strategy recovers more braking energy than the fuzzy control strategy, which verifies the superiority and rationality of the optimized strategy.

Acknowledgements

This study is partially supported by the National Natural Science Foundation of China (Grant No.51205051)

REFERENCES

[1] Sun, K.; Tao, L.; Miller, D.J. Vehicle emissions as an important urban ammonia source in the United States and China, *Environmental Science & Technology* 2017, 51(4), 2472-2481. https://doi.org/10.1021/acs.est.6b02805

[2] Cheng, M.; Tong, M.H. Development status and trend of electric vehicles in China, *Chinese Journal of Electrical Engineering* 2017, 3(2), 1-13. https://doi.org/10.23919/CJEE.2017.8048407

[3] Ajanovic, A.; Haas, R. On the economics and the future prospects of battery electric vehicles, *Greenhouse Gases: Science and Technology* 2020, 10(6), 1151-1164. https://doi.org/10.1002/ghg.1985

[4] Hu, J.J.; Guo, Z.H.; Peng, H. Research on regenerative braking control strategy of plug-in hybrid electric vehicle considering CVT ratio rate of change, *Proceedings of the Institution of Mechanical Engineers, Part D: Journal of Automobile Engineering* 2018, 232(14), 1931-1943. https://doi.org/10.1177/20954407017735681

[5] Saric, S.; Bab-Hadiashar, A.; Hoseinnezhad, R. Clamp-force estimation for a brake-by-wire system: A sensor-fusion approach, *IEEE Transactions on Vehicular Technology* 2008, 57(2), 778-786. https://doi.org/10.1109/TVT.2007.905251

[6] Ki, Y.H.; Lee, K.J.; Cheon, J.S. Design and implementation of a new clamping force estimator in electro-mechanical brake systems, *International Journal of Automotive Technology* 2013, 14(5), 739-745. https://doi.org/10.1007/S12239-013-0081-4

[7] Zhou, S.W.; Zhang S.Q.; Chen, Q.M. Vehicle ABS equipped with an EMB system based on the slip ratio control, Transactions of FAMENA, 2019, 43(SI-1), 1-12. https://doi.org/10.21278/TOF.43Si101

[8] Jo, C.; Hwang, S.; Kim, H. Clamping-force control for electromechanical brake, *IEEE Transactions on Vehicular Technology* 2010, 59(7), 3205-3212. https://doi.org/10.1109/TVT.2010.2043696

[9] Haggag, S.A.; Abidou, D. An approach to vehicle brake-by-wire optimal control tracking strategy, *SAE International Journal of Passenger Cars-Mechanical Systems,* 2013, 6(1), 154-162. https://doi.org/10.4271/2013-01-0686

[10] Grandone, M.; Naddeo, M.; Marra, D. Development of a regenerative braking control strategy for hybridized solar vehicle [J]. *IFAC-PapersOnLine* 2016, 49(11), 497-504. https://doi.org/10.1016/j.ifacol.2016.08.073

[11] Rajendran, S. Spurgeon, S.; Tsampardoukas, G. Intelligent sliding mode scheme for regenerative braking control, *IFAC-PapersOnLine*, 2018, 51(25), 334-339. https://doi.org/10.1016/j.ifacol.2018.11.129

[12] Oleksowicz, S.A.; Burnham, K.J.; Barber, P. Investigation of regenerative and anti-lock braking interaction, *International Journal of Automotive Technology* 2013, 14(4), 641-650. https://doi.org/10.1007/s12239-013-0069-0

[13] Khastgir S. The simulation of a novel regenerative braking strategy on front axle for an unaltered mechanical braking system of a conventional vehicle converted into a hybrid vehicle, *2013 Eighth International Conference and Exhibition on Ecological Vehicles and Renewable Energies (EVER)* 2013. https://doi.org/10.1109/EVER.2013.6521600

[14] Maia, R.; Silva, M.; Araújo, R. Electrical vehicle modeling: A fuzzy logic model for regenerative braking, Expert systems with applications, 2015, 42(22), 8504-8519. https://doi.org/10.1016/j.eswa.2015.07.006

[15] Nian, X.H.; Peng, F.; Zhang, H. Regenerative braking system of electric vehicle driven by brushless DC motor, *IEEE Transactions on Industrial Electronics* 2014, 61(10), 5798-5808. https://doi.org/10.1109/TIE.2014.2300059

[16] Sakai, S.I.; Sado, H.; Hori, Y. Dynamic driving/braking force distribution in electric vehicles with independently driven four wheels, *Electrical Engineering in Japan* 2002, 138(1), 79-89. https://doi.org/10.1002/eej.1113

[17] Driankov, D.; Hellendoorn, H.; Reinfrank, M. An introduction to fuzzy control, *Springer-Verlag Berlin Heidelberg* 1996, New York. https://doi.org/10.1007/978-3-662-03284-8

[18] Ferreira, A.A.; Pomilio, J.A.; Spiazzi, G. Energy management fuzzy logic supervisory for electric vehicle power supplies system, *IEEE transactions on power electronics* 2008, 23(1), 107-115. https://doi.org/10.1109/TPEL.2007.911799

[19] Biao, J.; Xiang, W.Z.; Yang, X.W. Regenerative Braking Control Strategy of Electric Vehicles Based on Braking Stability Requirements, *International Journal of Automotive Technology* 2021, 22(2), 465-473. https://doi.org/10.1007/s12239-021-0043-1

[20] Zhou, S.W.; Wang, Q.Y.; Liu, J.S. *Control Strategy and Simulation of the Regenerative Braking of an Electric Vehicle Based on an Electromechanical Brake*, Transactions of FAMENA, 2022, 46(1): 23-40. https://doi.org/10.21278/TOF.461019420

[21] Wang, M.; Li, Y.; Yuan, J. Comprehensive improvement of mixed-flow pump impeller based on multi-objective optimization, *Processes* 2020, 8(8), 905-918. https://doi.org/10.3390/pr8080905

[22] Heydari, S.; Fajri, P.; Rasheduzzaman, M. Maximizing regenerative braking energy recovery of electric vehicles through dynamic low-speed cutoff point detection, *IEEE Transactions on Transportation Electrification* 2019, 5(1), 262-270. https://doi.org/10.1109/TTE.2019.2894942

[23] Shukla, A.; Agarwal, P.; Rana, R.S. Applications of TOPSIS algorithm on various manufacturing processes: a review, *Materials Today: Proceedings* 2017, 4(4), 5320-5329. https://doi.org/10.1016/j.matpr.2017.05.042

[24] Liu, P.; Li, H.X. Fuzzy neural network theory and application, *World Scientific* 2004, Singapore. https://doi.org/10.1142/5493

[25] Kwan, H.K.; Cai, Y. A fuzzy neural network and its application to pattern recognition, *IEEE transactions on Fuzzy Systems* 1994, 2(3), 185-193. https://doi.org/10.1109/91.298447

[26] Singh, K.V.; Bansal, H.O.; Singh, D. Development of an adaptive neuro-fuzzy inference system–based equivalent consumption minimisation strategy to improve fuel economy in hybrid electric vehicles, *IET Electrical Systems in Transportation*, 2021, 11(3), 171-185. https://doi.org/10.1049/els2.12020

[27] Yang, Y.; Zhao, H.; Jiang, H. Drive train design and modeling of a parallel diesel hybrid electric bus based on AVL/Cruise, *World Electric Vehicle Journal* 2010, 4(1), 75-81. https://doi.org/10.3390/wevj4010075

[28] Liu, H.; Li, X.; Wang, W. Adaptive equivalent consumption minimisation strategy and dynamic control allocation-based optimal power management strategy for four-wheel drive hybrid electric vehicles, *Proceedings of the Institution of Mechanical Engineers, Part D: Journal of Automobile Engineering* 2019, 233(12), 3125-3146. https://doi.org/10.1177/20954407018816564

Submitted: 16.8.2022

Accepted: 06.7.2023

Shuwen Zhou
Jinshuang Liu*
Zhaolun Wang
Shaohua Sun
College of Mechanical Engineering and Automation, Northeastern University, Shenyang Liaoning, China
*Corresponding author:
liujinshuang@tom.com